ChemPhotoChem
Minireviews
doi.org/10.1002/cptc.202100180
Chemistry Europe
European Chemical Societies Publishing
www.chemphotochem.org

Special Collection

Time-Resolved X-Ray Spectroscopy to Study Luminophores with Relevance for OLEDs

Matthias Vogt[b] and Grigory Smolentsev*[a]

Organic light-emitting diodes (OLEDs) are employed in innovative display technologies and have the potential to be used widely in large area lighting. Luminophores containing 4d or 5d metals are efficient in electro-luminescent devices due to their phosphorescent properties but are scarce and expensive. Alternatives take advantage of temperature-activated delayed fluorescence (TADF), e.g. in Cu(I) complexes. We show modern X-ray spectroscopy methods exemplified on Ru, Ir and Cu-based luminophores offering insight into the capabilities of such techniques to researchers from various fields. Knowledge of structural rearrangements in the excited state is crucial to understand non-radiative energy losses and to develop efficient luminophores. Pump-probe X-ray absorption spectroscopy (XAS) gives information about the molecular structure in the excited state and the electronic structure. We show how this information can be complemented with X-ray emission spectroscopy at X-ray free-electron lasers (XFEL) and discuss the potential of time-resolved X-ray excited optical luminescence (TR-XEOL) to provide additional selectivity of XAS to luminescent sites.

1. Introduction

Organic light-emitting diodes (OLEDs) are electroluminescent (EL) units, which can be used not only in display applications but also in area lighting devices.[1] Currently, the OLED technology finds its way into a growing number of consumer products, such as smartphones, tablets, and TV screens due to its extraordinary properties exceeding the quality of concurrent established technologies e.g. liquid crystal displays (LCD). For instance, OLED displays offer superb image quality and contrast, a wide viewing angle, low weight, and energy efficiency as they do not require back-illumination.[2] Considering that lighting still consumes a significant amount of electrical power, OLEDs may hold promise for an energy-saving technology on a global scale.[3] Further, the unnecessary back-illumination can allow for the fabrication of extraordinary thin displays, with unprecedented flexibility in display and lighting designs.[1] As OLEDs can offer superior performance and enhanced energy efficiency at the same time it is not surprising that their development became a very active field of research in both academia[4–8] and industry.[9] For recent commercialized innovative products such as bendable panels and foldable devices see reference.[9]

A key material within an OLED is the luminescent dye within the emissive layer, where the efficiency of the exciton harvesting has great significance for the performance of the device. The electroluminescence is a consequence of electron-hole recombination in the emissive layer, forming singlet or triplet exciton. The simplest picture is that, for example, the hole is trapped first at the emitter complex and then the electron is attracted forming an excited charge-transfer state of the complex. Spins of the hole and the electron during such process can be combined into the singlet configuration (with total spin 0 and spin projection 0) or three triplet configurations (with total spin 1 and spin projection 1, 0 or −1). In a more complex picture, excitation can be formed in the emitter host material (organic semiconductor) and then transferred to the luminophore. In any case, either singlet or triplet excitons with a statistical distribution of 1:3 are formed.[10] Therefore, purely fluorescent organic dyes have a theoretical limit of 25% for the internal quantum efficiency (IQEmax) as only the singlet state is emissive. A prominent example of such emitters of the 1st generation OLEDs is aluminium tris(8-hydroxyquinoline) (**1** (Alq3), Figure 1A). In OLEDs of the second generation, the use of coordination compounds of rare precious metals, for instance, Ir, Pt, or Ru allows to overcome this limit and gave rise to highly efficient OLEDs. The ground state of such materials is typically singlet. Taking advantage of the "heavy atom effect", the metal center provides a large spin-orbit coupling enabling the efficient transition between singlet and triplet excited states (intersystem crossing, isc) as a prerequisite for photon emission via phosphorescence, which is probable in the case of strong spin-orbit coupling. Therefore, corresponding devices are regarded as PhOLEDs.[11] Such luminophores allow for a theoretical IQEmax of 100% as all generated excitons can be harvested (triplet harvesting). Large spin-orbit coupling constants of heavy metals may not be the exclusive parameter to govern the isc rate,[12] there are examples of heavy-atom-free organic compounds showing efficient isc.[13] Figure 1B shows

[a] Dr. G. Smolentsev
Energy and Environment Research Division,
Paul Scherrer Institute
Forschungsstrasse 111, 5232, Villigen-PSI (Switzerland)
E-mail: grigory.smolentsev@psi.ch
[b] Dr. M. Vogt
Fakultät für Naturwissenschaften II, Institut für Chemie,
Martin-Luther-Universität Halle-Wittenberg
Kurt-Mothes-Str. 2, 06120 Halle (Saale) (Germany)

Special Collection An invited contribution to the "GDCh and ChemPhotoChem: 5-Year Anniversary" Special Collection.

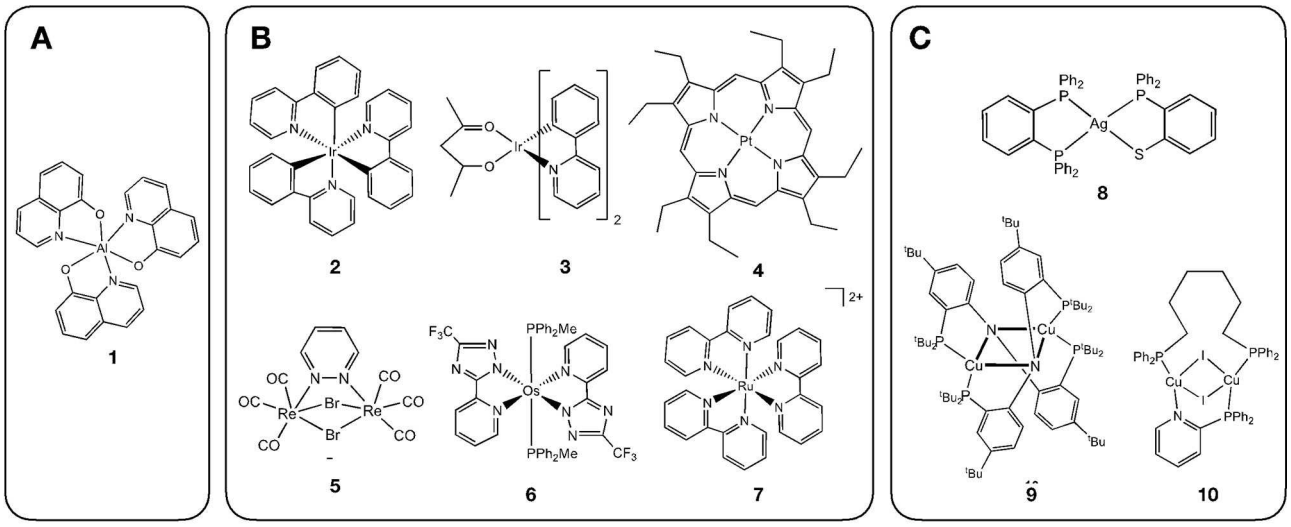

Figure 1. Examples of coordination compounds reported as luminescent dyes in OLEDs.[26] (**A**) fluorescent dye: Alq_3 (**1**) was one of the first compounds used for an OLED device.[27] **(B)** phosphorescent dyes (**2**–**7**): examples of well-known precious metal-based (Ir[28,29] and Pt[30]) emitters allowed for performant PhOLED devices, the example of the prominent $[Ru(bpy)_3]^{2+}$ dye (**7**),[31] (**6**) an example of an Os-based phosphorescent dye utilized in efficient OLEDs with orange emission,[32] (**5**) a rare example of a rhenium-based PhOLED emitter with high external quantum efficiency (EQE).[33] **(C)** TADF emitters (**8**–**10**): examples of Cu-based[34–36] and an Ag-based[37] complexes showing TADF-type emission.

exemplary phosphorescent emitter complexes with heavy precious metal centers (compounds 2–7). However, beyond the more obvious challenges regarding OLED device design, such as the requirement of high stability or the control of the emission wavelength, there is an intrinsic problem of PhOLEDs potentially hampering the growth of the OLED market sector. That is, the usage of rare precious metals, especially iridium, may impose a supply bottleneck.[14] Therefore, especially concerning the mass-manufacturing of large-area lighting panels,[15,16] it appears crucial to develop efficient emitting materials, which do not contain rare transition metal ions.[1,14] To increase the efficiency of OLEDs while avoiding rare-earth metals, a few alternative ideas were proposed including triplet-triplet annihilation,[17] hybridized local and charge transfer[18] and by side-stepping Kasha's rule.[19]

During the last decades, the 3rd generation of OLED emitters based on coordination entities with earth-abundant metal centers, mainly Cu, but also Ag[20–23] or entirely metal free[2,24] has appeared, taking advantage of the temperature-activated delayed fluorescence (TADF) effect[1,14,20,21,25]. In this regard, we want to specifically outline the compound class furnishing copper(I) metal centers as they will be the subject of further discussions within this review. Spin-orbit coupling is not strong in coordination entities with a lighter metal center, in particular, Cu; therefore, the emission is probable from the singlet state (fluorescence) and may be negligible from the triplet (phosphorescence). This behavior contrasts to Ir, Pt and other precious-metal-based emitters. The principle of TADF at photoluminescence and electroluminescence conditions is illustrated in Figure 2. For TADF materials the triplet state is long-lived and has a lifetime in the microsecond range. The energy difference between the singlet and the triplet states is so small that thermally activated reverse intersystem crossing (risc, T_1 to S_1 transition) is probable. This leads to emission from the singlet state (singlet harvesting) with a lifetime in the microsecond range and with a high quantum efficiency.[38]

The molecular designs for Cu-based dyes commonly aim for avoiding large structural rearrangements upon photo-excitation. A 'nested state' situation in which the ground and excited states have very similar geometry[39] may be favored because strong distortions often result in non-radiative decays[40] (Figure 2c) and can make the coordination sphere accessible for additional coordination inflicting direct quenching.[41] The majority of the reported investigations on Cu-based TADF materials are focused on three main compound classes: mononuclear Cu(I) complexes with tetrahedral coordination sphere[42–44] trigonally-coordinated mononuclear Cu(I) complexes[45,46] and multinuclear Cu(I) complexes with phosphine or nitrogen-containing ligands.[47,48] Dicoordinated linear Cu(I) complexes are also under investigation and are reported to possess extraordinary photoluminescence properties.[49,50]

The excited state usually has a metal-to-ligand charge transfer (MLCT) character. After such one-electron oxidation of Cu, mononuclear systems with tetrahedral coordination tend to adopt a flattened structure in the excited state due to Jahn-Teller distortions.[51,52] Therefore, the common strategy is to provide a rigid ligand framework of bulky ligands that make flattening and corresponding non-radiative losses less probable. Rigid structures can also be achieved for multinuclear complexes by profiting from the covalence of the copper core.[47] For trigonally-coordinated mononuclear complexes flattening distortions are impossible, which is an alternative strategy to minimize structural reorganization in the excited state and corresponding non-radiative energy losses.[45,53,54]

Synthetic efforts to produce novel luminophore-complexes are typically coupled with the characterization of materials by optical emission and absorption spectroscopy and time-

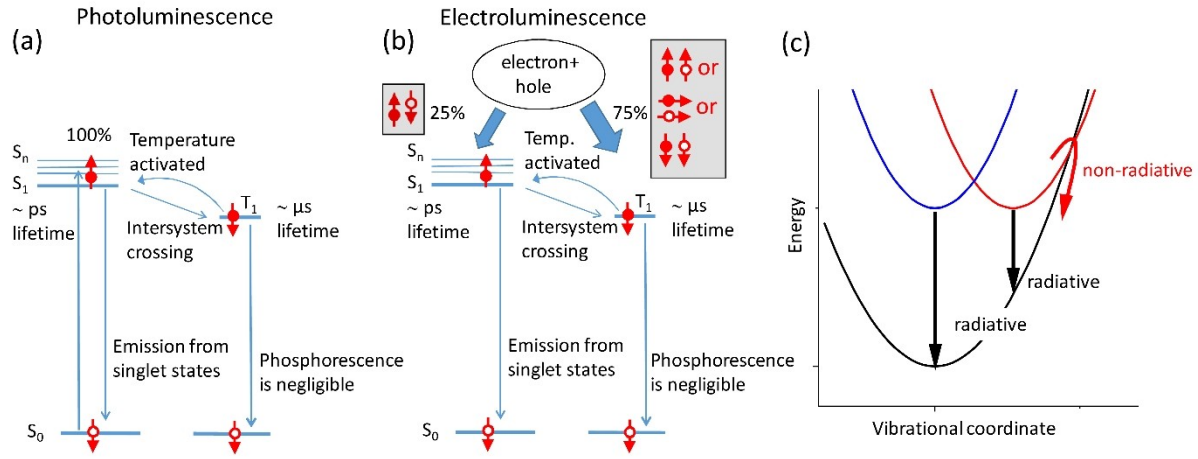

Figure 2. (a) Scheme of temperature-activated delayed fluorescence (TADF) as a result of photoexcitation; (b) the same scheme, but under electroluminescence conditions. The spin of electrons (holes) is shown as arrows with the full (empty) circles. S_0 is the ground state, S_1–S_n excited singlet states, T_1-excited triplet state. (c) Potential energy curves for the ground state (black line), the excited state which has the same structure as the ground state (blue line) and excited state with significantly different structure (red line). Non-radiative energy losses are probable if potential energy curves cross or if they are close to each other.

resolved emission decay measurements at ambient – and low (~77 K) temperatures.[55] Optical emission measurements provide direct information about energies and the quantum yield of radiative transitions. At low temperatures, the phosphorescence can become visible for materials showing TADF at room temperature. This allows to estimate the energy of both singlet and triplet states from the temperature-dependent emission spectra. A more precise estimation of energy separation between these states can be obtained by measuring the emission lifetime as a function of temperature assuming Boltzmann distribution for probabilities of the states. Nevertheless, the determination of the singlet-triplet energy splitting based on the measurements of emission decay at different temperatures is not always possible, because not only the probability of the transition from triplet to singlet excited state is temperature-dependent, but also non-radiative excited-state deactivation paths are strongly temperature-dependent.[21,25] Density functional theory (DFT) or time-dependent density functional theory (TDDFT) calculations are used to predict excited state energies and to interpret the spectra. Nevertheless, the computationally driven development of more efficient materials requires experimental verification of excited-state structural models that are used to predict both the energies of states and the probabilities of non-radiative deactivation processes.

The goal of this mini-review is to show how time-resolved X-ray spectroscopy can be used to investigate excited states of luminophores based on metal complexes that have relevance to OLED devices. Among different time-resolved techniques that cover the time range from sub-picoseconds to minutes, we will focus on methods using synchrotron radiation that cover the time range from 100 ps to microseconds, and highlight the first results and perspectives of experiments using X-ray free electron lasers.

2. Time-Resolved X-Ray Excited Optical Luminescence

In general, X-ray Excited Optical Luminescence (XEOL) is the effect where optical photons are emitted by a material after absorption of X-rays. Within the Time-Resolved X-ray Excited Optical Luminescence (TR-XEOL) method, the system is excited by monochromatic X-ray photons with energy scanned around the deep X-ray absorption edges (K, $L_{2,3}$ or M_3 corresponding to excitation of 1s, 2p or 3p atomic levels) of the participating elements, while for detection the optical luminescence is used. This luminescence is analyzed both spectrally (wavelength dependence) and kinetically (time dependence). In this way, the technique combines time-resolved optical photoluminescence measurements with X-ray absorption spectroscopy. In addition to that, for anisotropic systems (for example nanostructures or molecules arranged at the surface with preferred orientation) the linear polarization of synchrotron beams can be used to measure the polarization-dependent XEOL.[56,57]

The main elements of the setup are shown in Figure 3a. The luminescence wavelength dispersing element is typically a diffraction grating. Either a position-sensitive detector or a point detector, coupled with the data acquisition system, allows for the measurement of the relative time between X-ray pulses (bunches of the storage ring) and the detected optical photons (Figure 3b). XEOL detection can also be performed in total emission mode corresponding to the broad range of wavelengths, either using a separate detector or using zero-order reflection from the grating. A laser is not needed for TR-XEOL. The sample can be in the solid state or in solution,[58] but for OLED-related materials, such experiments were performed mainly in the solid state. In contrast to pump-probe spectroscopy, which we will discuss in the next section, the photoexcitation is not performed before the X-ray pulse; therefore the molecule, which is at the beginning in the initial ground

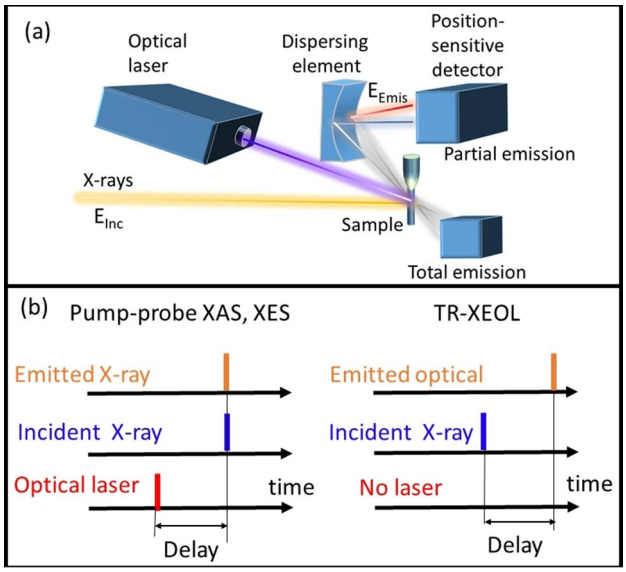

Figure 3. (a) Scheme showing the main elements of setups for time-resolved spectroscopic X-ray experiments. For pump-probe XAS the sample is excited by the laser and total X-ray emission/fluorescence is measured as a function of the energy of incident X-ray photons and delay between laser and X-ray pulses. For pump-probe X-ray emission, the incident energy is fixed, but the X-ray fluorescence is dispersed by a cylindrically curved crystal and measured as a function of the energy of emitted photons. For high-energy resolved fluorescence detection experiments (HERFD-XAS), the X-ray fluorescence is also dispersed and the signal at fixed emitted energy is measured as a function of incident energy. For TR-XEOL the optical luminescence is dispersed with a diffraction grating and a laser is not needed. (b) Scheme of the sequence of absorption and emission events for pump-probe XAS, XES and TR-XEOL experiments. For pump-probe experiments, the spectra are measured as a function of the delay between laser and X-ray pulses. The delay between absorption and emission of X-ray photons is negligible (~1 fs). For TR-XEOL the laser pulse is not needed and spectra are measured as a function of the delay between the incident X-ray pulse and the optical emission.

state, absorbs X-ray photon. The X-ray excitation decays through a cascade of processes, which include the inelastic scattering of photoelectrons and Auger electrons. Such scattering produces electrons of lower energy and shallower holes until the final radiative transition leads to electron-hole recombination and light emission. The relaxation pathways during XEOL, electroluminescence and photoluminescence processes are different. Nevertheless, in all these cases, as net result, one or only a few low-lying excited states are formed, for instance, a triplet MLCT state often is the most probable and relevant. For complexes with strong luminescence encompassing 4d or 5d transition metals, this state typically decays radiatively via the emission of optical photons. If the spectroscopic profile (position of the emission maximum, emission bandwidth, etc.) and the time-dependencies for the emission are similar for different excitation regimes (optical, X-ray or electrical), one can safely assume that the same excited states are formed. This gives the possibility to use TR-XEOL as a technique, which is exclusively selective for luminescent sites. Such selectivity can be applied for the separation of contributions into XAS spectra of "working/active" and "degraded" centers of luminescence, to understand the degradation mechanism. For example, the material can contain two sites with the same type of metal, but bear a different ligand sphere and only one of these two sites produces optical luminescence. In this case, the 'classical' XAS measurements in the fluorescence mode give an averaged spectrum of these two sites, while TR-XEOL can specifically give information about the luminescent center. Keeping this motivation in mind we will summarize what has been demonstrated for luminescent materials with relevance to the emissive layer in OLEDs utilizing the XEOL detection.

The TR-XEOL method was applied to luminescent materials with 4d and 5d transition metals including octahedral Ru(II) complexes with chelating homoleptic nitrogen-based (bipyridine and phenanthroline) donors,[60,61] Ru(II) compounds with slightly more complex mixed-N,P ligand spheres,[61] and *fac*-tris(2-phenylpyridine)iridium (*fac*-[Ir(ppy)$_3$])[62] in the soft, tender, and hard X-ray ranges.[63] For instance, when tris-(2,2-phenanthroline)ruthenium [Ru(phen)$_3$]$^{2+}$ was excited at the Ru K-edge the luminescent emission spectrum has two clearly separated features: the component associated to a maximum at 324 nm corresponds to the ligand-localized transitions, while the emission maximum at 613 nm originates from the MLCT state (Figure 4a). The component at 324 nm is rather short-lived, while a long-lived visible emission decays with a lifetime of 149 ns, which is expected for the MLCT phosphorescence (Figure 4b). The absorption spectrum at the Ru K-edge measured in photoluminescence mode (Figure 4c) is similar to spectra of related Ru complexes with an octahedral coordination sphere built by N-donor moieties.[59]

The situation gains more complexity at the Ru $L_{2,3}$ edges (Figure 4d). The L_3 absorption edge of Ru is close to the Cl K-edge and chloride ions are present in the material as counter-anions. Therefore, both edges are well seen when X-ray fluorescence detection (not the XEOL) is used. Counterions can influence the luminescence properties of electroluminescence devices based on Ru,[64] nevertheless, a strong emission from counterion is not expected for such Ru luminophores. Therefore, in the simplest picture, the Cl K-edge should be suppressed in the luminescence yield mode. In the experimental data one can see that Cl contributions are weaker, but still present (Figure 4 d, red trace). The decay of the excited state initially localized at Cl, leads to an energy transfer to the Ru center through various possible channels (X-ray fluorescence of Cl excites electrons of Ru, Auger electrons from Cl interact with the Ru center and participate in secondary processes, etc.). For the sample in the solid phase, the distance between Cl and Ru atoms is rather small and indirect luminescence induced by the excitation at Cl is not negligible. Such moderate selectivity of XEOL to the center excited by X-rays was observed via the detection of the optical luminescence in the broad wavelength- and in the full time range.

Ir(ppy)$_3$ (**2**) has been investigated using TR-XEOL in the soft (C and N K-edges)[62] and tender (Ir M_3 edge)[65] X-ray ranges. For soft X-rays, the absorption spectra measured using XEOL have inverted shapes (luminescence decreases when the incident X-ray energy is above the absorption edge) and the fine structure of the spectra, measured using the total electron and photoluminescence yields, are different. Sham and co-

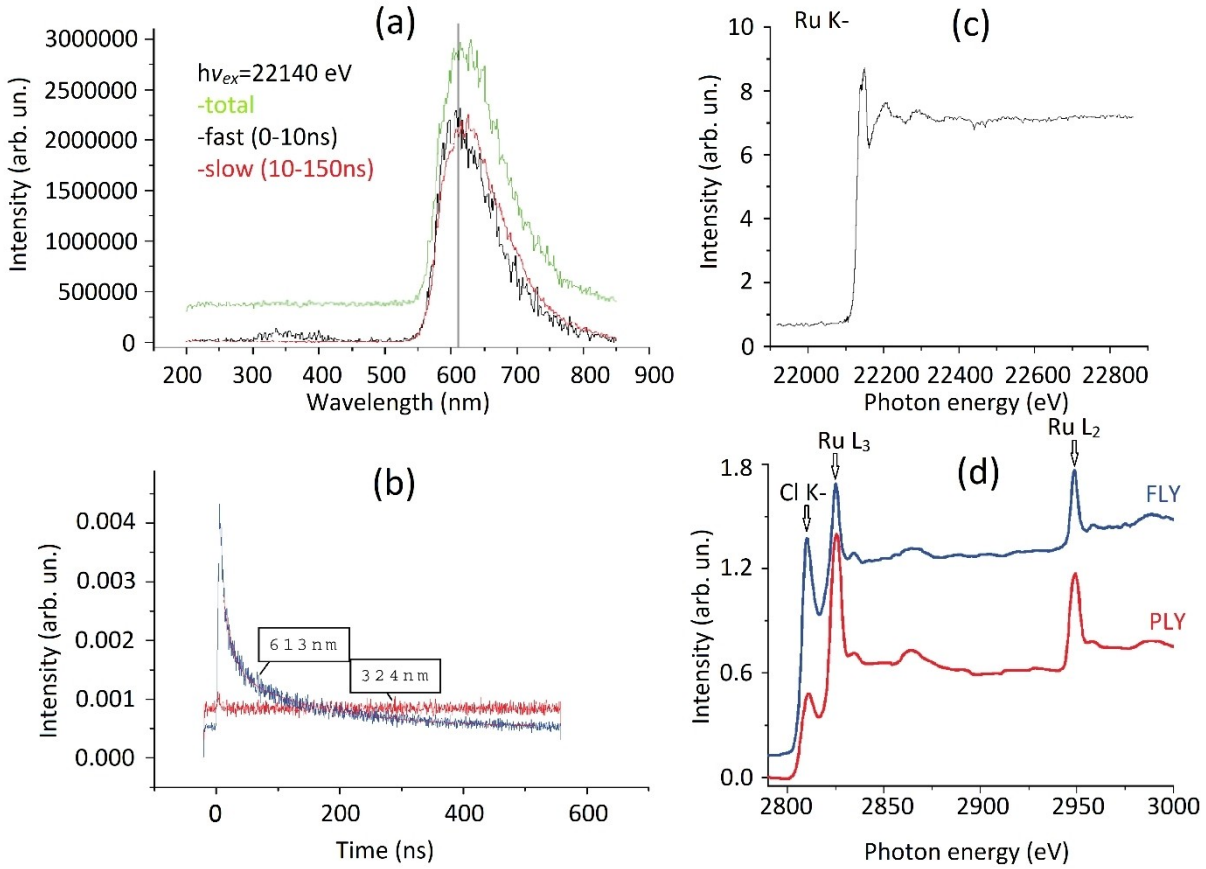

Figure 4. Results of TR-XEOL measurements from $[Ru(phen)_3]^{2+}$. (a) Time-gated optical luminescence spectra corresponding to fast (0–10 ns), slow (10–150 ns) and total time ranges. (b) Time-dependence of luminescence acquired at 613 (blue line) and 324 nm (red line) wavelengths. (c) Ru K-edge X-ray absorption spectrum measured in optical photoluminescence yield mode.[59] (d) Ru $L_{2,3}$-edge X-ray absorption spectra measured in the optical photoluminescence (red line) and X-ray fluorescence yield (blue line) modes. Adapted from Ref. [60] with the permission of AIP Publishing.

authors explain this observation by the difference of penetration depth of X-rays below and above the absorption edge that changes so significantly, that photoelectrons and Auger electrons do not completely thermalize for the excitation above the C K-edge, which leads to a lower photoluminescence quantum yield. A similar inversion effect, but with a smaller difference with respect to the shape of the spectra, was observed for the N K-edge of $[Ru(phen)_3]^{2+}$.[60] The Ir M_3 edge looks as expected, without inversion, but the background luminescence induced by the excitation of other atoms is strong.

Luminophores with lighter elements were also studied with XEOL. For instance, the spectra measured for Alq_3 (**1**) using optical luminescence detection at K-edges of Al, C, N and O are in reasonable agreement (no inversion was observed) with the data obtained using X-ray fluorescence and total electron yield detection.[63,66] The difference between $Ir(ppy)_3$ (**2**) and Alq_3 is the involvement of the metal in the photoluminescence process (after thermalization, the hole should be localized at Ir for $Ir(ppy)_3$ and mainly at C atoms for Alq_3). Such different behavior reflected within the spectra in the case of soft X-ray excitation, demonstrates the complexity of relaxation pathways leading to optical luminescence and that further fundamental investigations combining theory and experiment are required, to use this method as the site-selective probe. Phenomenological models that explain, in particular, the inversion of XEOL spectra were proposed in the early days of the development of this technique.[67,68] Later the approach was further developed and applied for the interpretation of XEOL-detected spectra using X-ray absorption spectra measured in transmission mode as the input and a set of varied parameters.[69] The approach can be also combined with well-developed methods for calculations of X-ray absorption spectra based on full multiple scattering theory,[70] DFT[71,72] or finite difference method.[73,74] Taking into account that light atoms (C, N, O) are often present in OLED materials in many different non-equivalent sites, the interpretation of spectra of these elements can be very complicated. For the hard X-ray range, the number of experimental TR-XEOL data published is very limited, but it seems that the initial creation of an electron vacancy at the same atom where the hole is located in the triplet MLCT state simplifies the situation. Therefore, TR-XEOL in the hard X-rays regime looks promising as a method to probe selectively luminescent MLCT sites of metal complexes.

3. Pump-Probe XAS Study of Mononuclear Cu Complexes

The TR-XEOL method described in the previous section allows to use the time-dependence of the optical luminescence as one of the criteria to get selectivity to atomic sites of interest. Nevertheless, it does not allow the investigation of the photo-excited sites because X-ray photons interact with complexes in the ground state simultaneously exciting them. Within the pump-probe X-ray method, the system is first excited with an optical pump and then probed with an X-ray pulse for different delays between these two pulses (Figure 3). Spectra are measured as a function of energy of incident X-ray photons. Due to the sensitivity of the X-ray absorption spectrum to the local atomic structure, one can get detailed information about structural changes in the excited state. The method does not require any long-range order of the system and in combination with the large penetration depth of hard X-rays (~1 mm), this makes pump-probe XAS a unique method to investigate the atomic structure of the excited states of metal complexes in solution.[76] XAS is also sensitive to some details of the electronic structure, in particular, the oxidation state of metals can be determined,[77,78] which can be complemented by X-ray emission experiments that are sensitive to both spin and oxidation states.[76,79–81] Depending on the required time resolution, pump-probe XAS data acquisition can be performed at synchrotron sources by gating the detector to one X-ray pulse (which allows getting ~100 ps resolution)[82,83] or by measuring the arrival time of many X-ray pulses (pump-sequential-probes method with ~20 ns resolution).[84] At X-ray free electron lasers experiments can be performed in the time range which starts from tens of femtoseconds, which is possible due to shorter X-ray pulses.[80] There are also other techniques to produce such ultrafast X-ray pulses, including slicing[85] low-α and coherent harmonic generation at synchrotrons,[86] high harmonic generation,[87] plasma sources[88] and betatron sources[89] at lasers. In comparison to X-ray FELs these techniques provide lower X-ray flux at the sample. While some of these techniques had pioneering roles when X-ray FELs were not available, now these techniques are redefining their niche in the landscape of ultrafast X-ray techniques. For materials with potential use in OLEDs involving the TADF effect, a few ps delays between optical and X-ray pulses are required to probe the singlet excited state, while the time range 10 ns – 1 μs is of particular importance since the triplet excited state is typically observed in this time interval.

The homoleptic Cu complex $[Cu(dmp)_2]^+$ (dmp = 2,9-dimethyl-1,10-phenanthroline) is one of the first materials in which the TADF effect was discovered,[90] but according to the current standards, this complex is not so efficient (the emission quantum yield is ~$2*10^{-4}$ in CH_2Cl_2 at room temperature).[24,90] The structure of this complex in the triplet excited state was investigated in pioneering XAS experiments,[52,91] later $[Cu(dmp)_2]^+$ and its derivatives were further investigated utilizing pump-probe X-ray spectroscopy.[75,92–96] A previous review[97] summarizes early progress in this field and we will focus on the findings reported in recent articles.[75,94,98,99] For homoleptic diimine Cu(I) complexes, the photoexcitation induces Jahn-Teller distortions around the metal center and the initially tetrahedral configuration flattens. This can open the metal atom environment to accommodate an additional ligand in five-fold coordination. The degree of flattening distortions and how easily the fifth ligand can reach the metal depends on the substituents at the 2,9 positions of the phenanthroline. The recent analysis of the fine details of the Cu K-edge transient X-ray absorption spectrum has identified the features of the spectrum that allow for distinguishing between four- and five-coordinated Cu(II) centers.[98] In particular, the pre-edge peak associated with the transition to the d-vacancy of Cu(II) can be observed only for the four-coordinated geometry and it has a very weak intensity if the interatomic distance between Cu and the fifth ligand is less than 2.2 Å. For $[Cu(dmp)_2]^+$ the five-coordinated geometry is realized for electrochemically oxidized Cu(II) while after photoexcitation only a four-coordinated geometry is observed experimentally.[92,98] The exciplex, which is formed as a result of the interaction between the solvent and the photoexcited complex in the triplet state, can be involved in the relaxation processes only as a short-lived state, which decays faster than it forms. In this way, solvents influence the excited state lifetime. For derivative complexes with sec-butyl and n-butyl groups in the 2,9-positions of phenanthroline, it has been found that Cu atoms remain four-coordinated after photoexcitation[75,98] This can be concluded from the comparison of the experimental transient pump-probe spectra and the theoretical differences between the spectra of excited triplet – and singlet ground state (Figure 5). Calculations were performed for DFT-optimized four-coordinated and five-coordinated models with additional solvent (acetonitrile) coordination. Theoretical spectra agree with the experiment only for four-coordinated model.

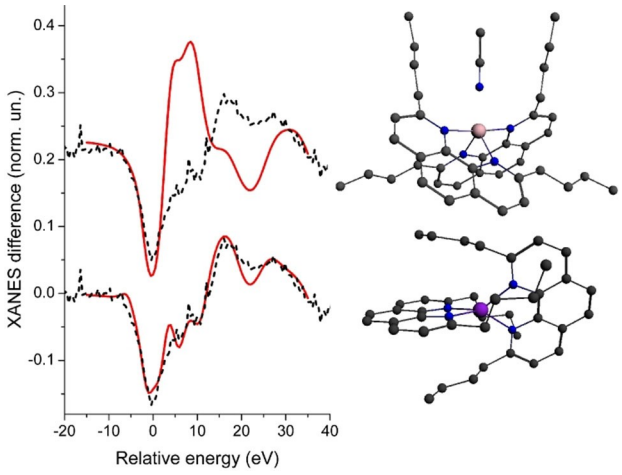

Figure 5. Theoretical difference spectra (red, solid) between Cu K-edge XANES of triplet excited and singlet ground states of $[Cu(dbp)_2]^+$, compared to the experimental difference spectra between photo-excited and unexcited state of $[Cu(dbtmp)_2]^+$ (black, dashed). Corresponding models of the excited state are also shown. Reproduced under terms of the CC-BY license from Ref. [75], copyright 2013, the Authors, published by the American Chemical Society.

The copper site can be additionally coordinated in the excited state not only by the solvent molecule but also intramolecularly by suitable coordinating moieties present in the ligand scaffold. For example, for related derivatives of $[Cu(dmp)_2]^+$ with $-CH_2OCH_3$ or $-CH_2SCH_3$ in the 2 and 9 position of the phenanthroline ligand, five-coordinated excited states were observed (Figure 6a).[94] Naturally, a –OMe or –SMe donor, respectively, of one of the substituents is pre-aligned closely to the Cu center already in the ground state and after photoexcitation the corresponding distances became shorter: Cu–O 2.29 Å and Cu–S 2.47 Å. Notably, related heteroleptic Cu complexes with diphosphino and 2,9-disubstituated phenanthroline ligand set, that is $[(xant)Cu(Me_2phenPh_2)]PF_6$ (xant = xantphos, $Me_2phenPh_2$ = bathocuproine) and $[(xant)Cu(R_2phen)]PF_6$, where R = 2,9-CH_2OCH_3 or CH_2SCH_3, were also investigated with pump-probe XAS.[94,99] However, these related complexes with the same phenanthroline substituents in 2 and 9 positions (i.e. $-CH_2OCH_3$ or $-CH_2SCH_3$) do not form the five-coordinated excited state (Figure 6b). Moreover, the Cu–P interatomic distance increases significantly after photoexcitation, which can lead to dissociation of the ligand after some excitation cycles leading to material instability and formation of homoleptic complexes in solution.

4. Multinuclear Cu Complexes: Complementarity of Pump-Probe X-Ray Techniques

In this section, we will discuss the complementarity of three pump-probe X-ray techniques: X-ray absorption, X-ray emission (XES) and wide-angle X-ray scattering. X-ray emission spectra are measured as a function of the energy of photons emitted by the sample, which requires a dispersive element, for example a cylindrically bent crystal for the spectrometer with von Hamos type geometry. The energy of the incident X-ray beam is fixed for such experiments. X-ray emission spectra correspond to the electron transitions between core levels but have sensitivity to the charge and spin state of the studied element due to the screening of core levels by the electron density of valence electrons, the exchange interaction between valence and core electrons and multiplet effects.[100] Measurements of X-ray scattering require a 2D detector placed after the sample to register photons scattered in the wide angular range. The scattering pattern is defined by the distribution of electron density and therefore in the pump-probe configuration this method allows to monitor photoinduced movements of parts of the molecule with large electron density, for example, displacements of heavy atoms.

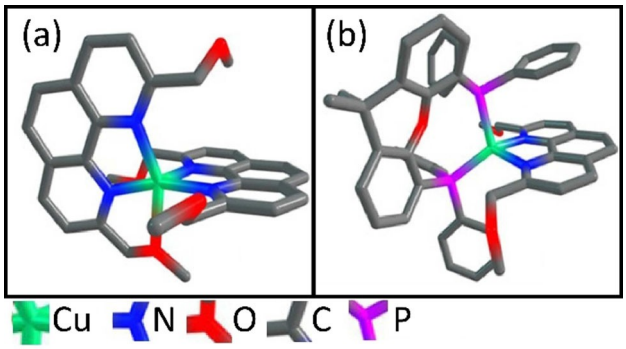

Figure 6. The structure of triplet excited state of $[Cu(R_2phen)_2]^+$ (a) and $[(xant)Cu(R_2phen)]$ (b) where R = CH_2OCH_3. Adapted from Ref. [94] with the permission of John Wiley and Sons, copyright 2020.

Multinuclear Cu complexes provide a versatile platform for the development of luminophores in OLEDs due to the possibility to minimize structure rearrangement in the excited state and thus also minimize associated non-radiative energy losses as the rigid structure may be established benefiting from strong Cu–Cu interactions in the multinuclear core. At the same time, photophysical processes in such materials can be much more complex in comparison to mononuclear compounds and therefore theoretical predictions should be verified by the experiment. By discussing the example of the cationic small organometallic cluster $[Cu_4(PCP)_3]^+$ (PCP = 2,6-$(PPh_2)_2C_6H_3$), we will demonstrate how different pump-probe X-ray techniques can uniquely provide complementary information about the electronic and local atomic structure in the triplet excited state. The chemical structure of the tetra-nuclear cluster $[Cu_4(PCP)_3]^+$ is shown in Figure 7a. This complex demonstrates strong green emission in solution (with a maximum at 525 nm and FWHM of 60 nm in tetrahydrofuran) and in the solid state. Detailed temperature-dependent measurements of the photoluminescence, its lifetime as well as the DFT predictions of orbitals involved in the luminescence are reported in.[47] The ground-state structure is known from a single crystal X-ray diffraction study.[47] Four Cu atoms form a slightly non-planar diamond-like structure with diagonal Cu–Cu distances of 2.32 Å and 4.72 Å. There are two types of Cu atoms, those coordinated by three P donors (P domain) and those with linear coordination by two carbanions (C domain), whereby one phenylate ring serves as a bridge between the two Cu (Cu1 and Cu4) atoms of the C domain.

Naturally, various questions arise concerning the excitation and the associated charge transfer process of this multi-core compound with different donor set (P, C) domains. For instance: 1) Which Cu atoms, C- or P-coordinated, are involved in the charge transfer? 2) What is the role of the phosphine ligands, more precisely, do they solely keep the structural integrity/rigidity of the cluster or do they actively participate in the charge transfer? 3) How pronounced are the structural changes in the excited states? Detailed knowledge about the structural changes is of importance because they strongly influence the probability of non-radiative losses and therefore photoinduced distortions are directly linked with the quantum efficiency of the luminescence. Furthermore, the experimental data about charge redistribution can be used to verify or calibrate computation methods for the rational design of even more complex luminescent materials.

Three pump-probe X-ray techniques, namely X-ray absorption spectroscopy near Cu K-edge, X-ray emission spectroscopy at the P Kα line and solution-state X-ray scattering were used

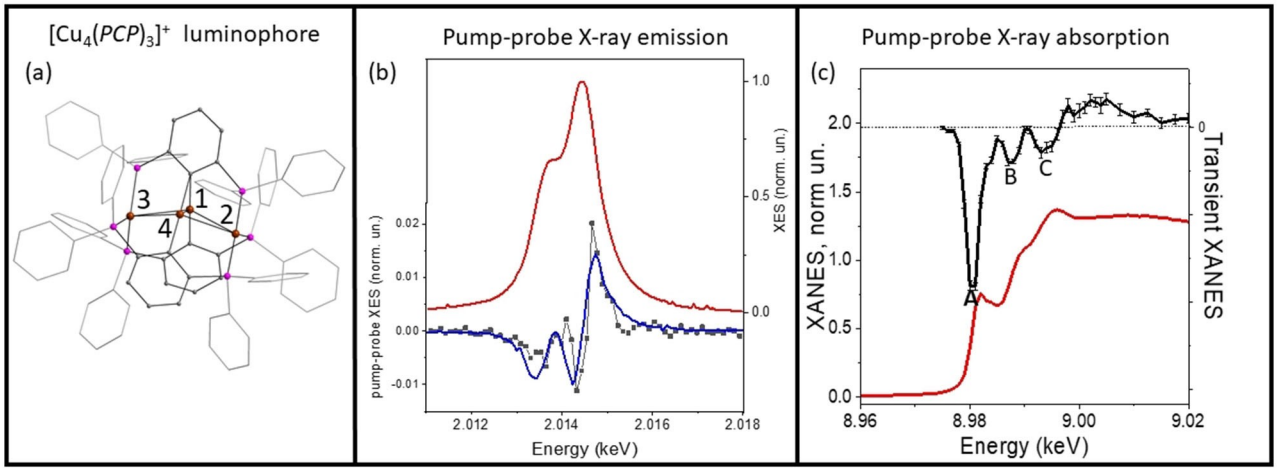

Figure 7. (a) Multinuclear luminophore $[Cu_4(PCP)_3]^+$ (PCP = 2,6-$(PPh_2)_2C_6H_3$). Cu atoms are orange, P atoms are violet and C atoms are grey. H atoms are omitted for clarity. (b) P K_α X-ray emission spectrum of $[Cu_4(PCP)_3]^+$ in the ground state (red line), pump-probe X-ray emission spectrum corresponding to the transition to triplet excited state (black line) and the signal calculated from the expected shift of emission lines (blue line). (c) Cu K-edge X-ray absorption spectrum for the ground state (red line) and pump-probe X-ray absorption spectrum (black line) corresponding to 1 μs time window after photoexcitation. Adapted under terms of the CC-BY license from Ref. [101]. Copyright 2020, The Authors, published by Springer Nature.

to investigate the $[Cu_4(PCP)_3]^+$ cluster upon photo-excitation in solution.[101] The experimental data allowed to address the above-mentioned questions for the triplet excited state. The results of the pump-probe X-ray absorption measurements are presented in Figure 7c. Spectra have been acquired using the pump-sequential-probes method at the *SuperXAS* beamline of the *SLS* synchrotron. Similar to the case of the mononuclear Cu complexes the negative maximum of the transient signal *A* (at *ca.* 8.98 keV) is an indication of Cu oxidation. Moreover, calculations of XANES demonstrated that the absorption maxima for C- and P-coordinated sites are shifted in energy and therefore, changes of the local charge at different types of Cu atoms induce features in the transient spectra that are also energy-shifted. The oxidation of C-coordinated Cu atoms produces feature *C*, the oxidation of P-coordinated Cu atoms induces feature *B* (Figure 7c). The fact that both features are observed experimentally indicates that both types of Cu atoms participate in the charge transfer induced by the transition to the triplet excited state.

To clarify the role of the phosphorus atoms a pump-probe XES experiment has been performed at the X-ray Free Electron Laser *SwissFEL*. Changes of the charge on the phosphorus atoms lead to an energy shift of both XES maxima. The shift of each peak is seen as one negative peak followed by one positive peak for higher oxidation state (formal charge) in the triplet state. Therefore, in this case, the transient spectrum is represented by two negative and two positive peaks (Figure 7b). From the amplitude of the transient signal, it has been estimated that the average formal charge of P atoms changes by more than 0.097 electrons.

Pump-probe X-ray scattering in solution is a technique sensitive to the relative movements of parts of the molecule with large electron density induced by photoexcitation. Therefore, this technique has been used to verify structural differences between singlet and triplet states. This sensitivity is especially pronounced in the region of high values of momentum transfer Q 2.0–6.5 $Å^{-1}$ while the pump-probe scattering signal in the region of low momentum transfer Q (below 2.0 $Å^{-1}$) has significant contributions from other effects such as laser-induced heating and density changes of the solvent. The comparison of the experimental scattering signals with theoretically calculated ones derived from DFT-based optimized structures of the singlet and triplet states of $[Cu_4(PCP)_3]^+$ allowed us to verify the suggested structural model, in particular, the small (0.05 Å) elongation of the Cu–Cu bond for C-coordinated sites and shortening by 0.12 Å of the distance between P-coordinated Cu atoms. Moreover, the information about the changes of charge of the P atoms from the XES experiments and about the involvement of both types of Cu atoms into the charge transfer from XAS, allowed us to compare different basis sets and exchange-correlation potentials used at different levels of DFT theory. In this way, pump-probe X-ray techniques provide valuable experimental input for the validation and verification of theoretical methods, that can be used in the future for the computational prediction of potent emitter materials.

5. Pump-Probe XAS Study of Ir-Based Luminescent Materials

For phosphorescence OLEDs (PhOLEDs) the quantum efficiency of the light emission is typically very high because of the strong spin-orbit coupling provided by the presence of heavy atoms. Therefore, the development of luminophores is centered on two main aspects: 1) Tuning the energy of states involved in the light emission to obtain the required color of emission and to match the energies of the host material. In particular, stable PhOLEDs with clear blue color are still a challenge.[102] 2) The

reduction of the lifetime of the triplet excited state. This is important because at electroluminescence conditions, corresponding to high brightness, the concentration of complexes in the triplet state can be high and triplet-triplet annihilation can reduce the efficiency of light emission.[103] The probability of this process reduces if the triplet lifetime is shorter, but of course, such decay should be radiative.

Using pump-probe X-ray spectroscopy one can obtain information about the energies of molecular orbitals in both ground-state singlet and excited-state triplet. Due to the localization and symmetry of the excited core level, the projection that is seen using XAS is specific and has a higher selectivity, in comparison to optical absorption. For example, for the L_3 edge of Ir, the projection to the d-states of the metal is dominant, so unoccupied 5d-states of Ir are directly probed and additional information about the metal environment comes from more delocalized d-states of the continuum. In this way, X-ray and optical spectroscopy provide complementary information looking at different projections of the electronic density of states.

If the structural rearrangements within the luminescent material are small, which is the case for many Ir-based materials, the $L_{2,3}$ pump-probe X-ray absorption spectra are mainly induced by the changes of the electronic structure which accompany the photoexcitation. The core-hole lifetime of Ir 2p levels is relatively large (4.94 eV), which influences the broadening of X-ray absorption spectra. By measuring X-ray absorption spectra in the fluorescence mode, but with high energy resolution for fluorescent photons, it is possible to enhance the energy resolution by eliminating the contribution of the 2p level.[79,100] This became possible due to the resonance nature of the process, which leads to the broadening of the spectrum to 3d level width (which corresponds to the final core-hole) instead of an intermediate 2p hole. The technique is called high energy-resolved fluorescence detection (HERFD) and it requires an additional X-ray emission spectrometer. While this method is used in the steady-state regime for three decades,[105] first pump-probe HERFD measurements have been demonstrated only recently.[106] Pump-probe spectra of $[Ir^{III}(ppy)_2(bpy)]^+$ (where ppy = 2-phenylpyridine and bpy = 2,2′-bipyridine) after photoexcitation were measured for this complex in pure CH_3CN solution and as a part of a multicomponent system for hydrogen evolution. A picosecond XAS experiment was also performed for $Ir(ppy)_3$, but with total fluorescence yield detection.[107] Pump-probe spectra of $[Ir(Chpy)_2(dtbbpy)]PF_6$ containing two chromenopyridinone and one bipyridine-based ligand were also reported[104] and shown in Figure 8.

The shape of the ground state XANES and pump-probe spectra of pseudo-octahedral Ir complexes with light atoms (N, C) in the first coordination shell are similar and can be qualitatively interpreted in the same way. Such description can be confirmed by theoretical DFT-based calculations (dashed lines at Figures 8a and b), which were performed using the previously developed method.[72] Such interpretation is qualitatively summarized in Figure 8c. In the ground state, the oxidation state of Ir is 3+. In the pseudo-octahedral environment, t_{2g} levels are fully occupied while e_g orbitals are completely empty. The main maximum of the absorption spectrum around 11220 eV corresponds to the transition of 2p electron to these e_g states. Photoexcitation of the Ir center leads to the transition of an electron from t_{2g} level to a molecular orbital which mainly has ligand character and therefore is not visible in XAS. The vacancy at e_g states can be

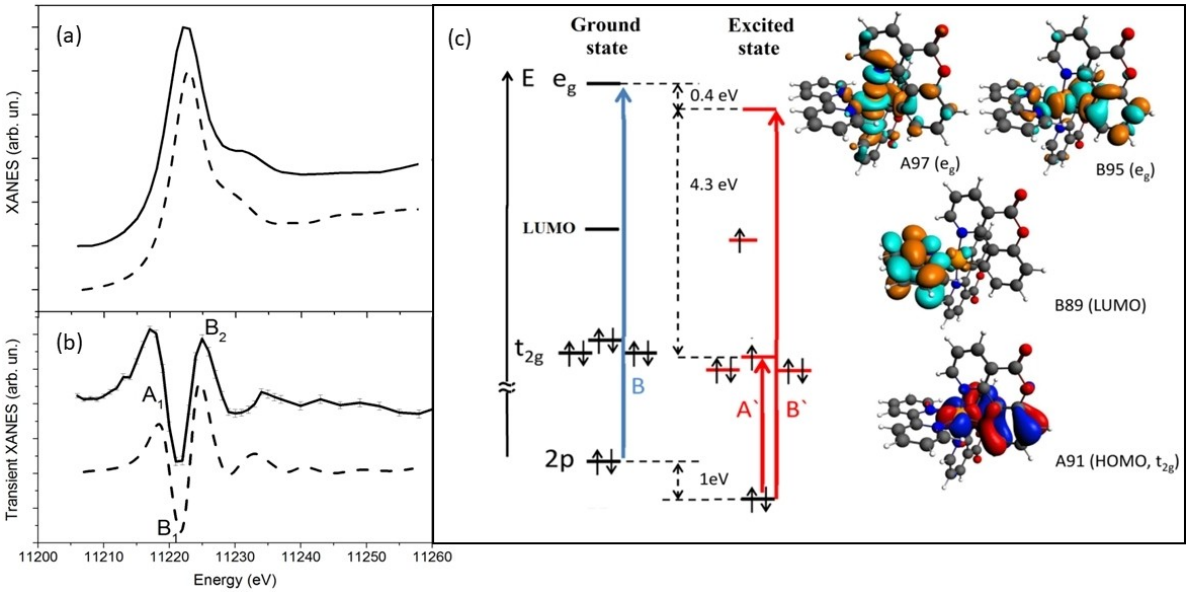

Figure 8. (a) Ir L_3 XANES spectra of $[Ir(Chpy)_2(dtbbpy)]^+$ in the ground state obtained experimentally (solid line) and using DFT-based theoretical calculations (dashed line). (b) Transient XANES spectra obtained experimentally (solid line) for a 1 μs time window and using DFT-based calculations (dashed line). (c) Energy level diagram and some important molecular orbitals which are relevant to explain transient Ir L_3 XANES spectra. Adapted from Ref. [104] with permission from the Royal Society of Chemistry.

well observed in XAS and therefore, the photoexcitation leads to the appearance of positive peak A_1 of the transient XAS spectrum (Figure 8b). At the same time, the screening of levels localized at the Ir center, including both 2p- and 5d-, also changes. The 2p-levels move down in energy a bit more than the 5d-levels for the $5d^5$ configuration. Therefore, the position of e_g relative to the 2p states changes towards higher energies after photoexcitation, which is seen as the negative peak B_1 and positive peak B_2 in the transient XAS spectrum.

The results of the investigations of Ir-based materials, summarized above, demonstrate the sensitivity of pump-probe XAS spectra to the electronic structure changes even in the case of very small structural rearrangements (<0.02 Å for the Ir-ligand distances). The width of Ir $2p_{3/2}$ state is 4.94 eV, therefore enhancing the energy resolution using pump-probe HERFD technique is promising to resolve fine details of 5d level splitting. For the example described above, which was measured using total fluorescence mode, and for $[Ir^{III}(ppy)_2(bpy)]^+$ previously studied with HERFD[106] the energy splitting of 5d levels is large, it can be well described with octahedral field model and therefore both detection modes provide similar information. The pump-probe HERFD can have advantages for ligand environments producing more complex splitting of Ir energy levels. Nevertheless, the requirement of an additional X-ray emission spectrometer for HERFD experiments reduces the detection efficiency by a few orders of magnitude and therefore the accumulation of sufficient statistics of pump-probe transient spectra is often a challenging task. In addition to the energy resolution and statistics of photons, that benefit from instruments with high X-ray flux, the X-ray induced damage has to be taken into consideration, especially for samples available in small quantities. Looking from another perspective, materials with the large splitting of d-states are very relevant: blue phosphorescent emitters show increased emitting-state energy, the corresponding MLCT states may arise close to the metal-centered (MC) d-d excited state resulting in emission quenching or even structural changes of the complex, e.g. ligand dissociation.[108,109] Such ligand release from the MC state has been investigated with pump-probe X-ray techniques for **cis**-$[Ru(bpy)_2(py)_2]^{2+}$.[110] Moreover, pump-probe XAS has been used to investigate the interplay of MLCT and MC states during excited state decay using XFELs[111,112] While these investigations of Fe complexes have mainly fundamental character and such materials do not find direct applications in OLEDs, they demonstrate the possibility of this technique. Therefore pump-probe X-ray spectroscopy can be a very valuable tool that may find value for the development of blue PhOLEDs and their future investigations with respect to both, their electronic structure and their excited state structural rearrangements.

6. Outlook

Coupled with the increased number of X-ray free electron lasers available worldwide and the growing diversity of specialized instruments at such facilities, pump-probe X-ray absorption and X-ray emission experiments are currently more accessible than in the previous decade. The pump-probe X-ray emission experiment described above for the small cluster $[Cu_4(PCP)_3]^+$ benefited mainly from a high number of photons per pulse at the XFEL in comparison to synchrotron facilities, as well as from the setup optimized for the tender X-ray range. Another feature of the XFEL that is widely used for pump-probe experiments is the short pulse duration. In the context of the investigation of OLED luminophores, it allows to catch the singlet excited state. Indeed, for TADF materials this state is relevant because light emission occurs from this state. Non-radiative decays from this state can also reduce the quantum efficiency of the material and therefore the control of structural rearrangements in the singlet excited state is crucial. The singlet state is short-lived with a typical lifetime of a few ps, which is shorter than the duration of a single X-ray pulse at the synchrotron (~100 ps) and therefore, typically, it cannot be probed at synchrotron radiation facilities. At electroluminescence conditions, the singlet state will be extremely difficult to observe because the reverse intersystem crossing is much slower than the radiative decay of the singlet state (Figure 2b). Therefore, pump-probe experiments at XFELs provide a unique and straightforward way to probe the singlet excited state of OLED materials and we expect growth in this direction of research.

Another strategic direction for X-ray spectroscopic experiments on OLEDs is the transition from the investigation of luminophores as complexes in solution towards the study of these materials directly in the electroluminescent devices or their prototypes. Operando investigations of electrochemical materials[113] or rechargeable batteries[114,115] are very common at synchrotron facilities and related experiments on OLEDs can be technically quite similar. In particular, such measurements may shed light on degradation processes occurring in OLEDs devices with time by comparing the structure of fresh and damaged luminophores using X-ray absorption spectroscopy. A combination of traditional fluorescence detection and TR-XEOL could be used for such experiments. In particular, the device with $[Cu_4(PCP)_3]^+$ luminophore can be interesting for such applications. Additional selectivity to luminescent sites provided by TR-XEOL will be very beneficial to separate XAS changes that do not lead to noticeable emission change from effects that lead to the degradation of the luminophore. Pump-probe experiments at synchrotrons on photoluminescent devices are challenging. The reason is the high repetition rate of the laser pulses (and therefore average laser power) which in combination with a limited area of the device (~cm^2) can lead to quick laser-induced damage (or at least perturbation and overheating of the device). It is more likely that such experiments can be performed at a low repetition rate (~100 Hz) XFELs because the laser power for such experiments is ~3 orders of magnitude lower than at synchrotrons due to the difference in repetition rates. However, even if the powerful X-ray pulses damage the material at XFELs, it is possible to establish a scan over a large enough area of the device to have fresh spots for a sufficiently long period of statistic accumulation.

Acknowledgements

Open access funding provided by ETH-Bereich Forschungsanstalten.

Conflict of Interest

The authors declare no conflict of interest.

Keywords: Copper · light emitting diodes · luminophores · pump-probe spectroscopy · x-ray absorption spectroscopy

[1] D. Volz, M. Wallesch, C. Fléchon, M. Danz, A. Verma, J. M. Navarro, D. M. Zink, S. Bräse, T. Baumann, *Green Chem.* **2015**, *17*, 1988–2011.
[2] M. Y. Wong, E. Zysman-Colman, *Adv. Mater.* **2017**, *29*, 1605444–1605444.
[3] A. Nardelli, E. Deuschle, L. D. de Azevedo, J. L. N. Pessoa, E. Ghisi, *Renewable Sustainable Energy Rev.* **2017**, *75*, 368–379.
[4] K. Dhbaibi, L. Abella, S. Meunier-Della-Gatta, T. Roisnel, N. Vanthuyne, B. Jamoussi, G. Pieters, B. Racine, E. Quesnel, J. Autschbach, J. Crassous, L. Favereau, *Chem. Sci.* **2021**, *12*, 5522–5533.
[5] F. Ni, C.-W. Huang, Y. Tang, Z. Chen, Y. Wu, S. Xia, X. Cao, J.-H. Hsu, W.-K. Lee, K. Zheng, Z. Huang, C.-C. Wu, C. Yang, *Mater. Horiz.* **2021**, *8*, 547–555.
[6] A. S. Romanov, S. T. E. Jones, Q. Gu, P. J. Conaghan, B. H. Drummond, J. Feng, F. Chotard, L. Buizza, M. Foley, M. Linnolahti, D. Credgington, M. Bochmann, *Chem. Sci.* **2020**, *11*, 435–446.
[7] D. Di, A. S. Romanov, L. Yang, J. M. Richter, J. P. H. Rivett, S. Jones, T. H. Thomas, M. A. Jalebi, R. H. Friend, M. Linnolahti, M. Bochmann, D. Credgington, *Science* **2017**, *356*, 159–163.
[8] Y. Wu, C. Yang, J. Liu, M. Zhang, W. Liu, W. Li, C. Wu, G. Cheng, Q. Yang, G. Wei, C.-M. Che, *Chem. Sci.* **2021**, *12*, 10165–10178.
[9] G. Hong, X. Gan, C. Leonhardt, Z. Zhang, J. Seibert, J. M. Busch, S. Bräse, *Adv. Mater.* **2021**, *33*, 2005630–2005630.
[10] H. Yersin, A. F. Rausch, R. Czerwieniec, T. Hofbeck, T. Fischer, *Coord. Chem. Rev.* **2011**, *255*, 2622–2652.
[11] P.-T. Chou, Y. Chi, *Chem. Eur. J.* **2007**, *13*, 380–395.
[12] M. Chergui, *Dalton Trans.* **2012**, *41*, 13022–13029.
[13] J. Zhao, K. Chen, Y. Hou, Y. Che, L. Liu, D. Jia, *Org. Biomol. Chem.* **2018**, *16*, 3692–3701.
[14] C. Bizzarri, E. Spuling, D. M. Knoll, D. Volz, S. Bräse, *Coord. Chem. Rev.* **2018**, *373*, 49–82.
[15] J. W. Park, D. C. Shin, S. H. Park, *Semicond. Sci. Technol.* **2011**, *26*, 034002.
[16] M. Eritt, C. May, K. Leo, M. Toerker, C. Radehaus, *Thin Solid Films* **2010**, *518*, 3042–3045.
[17] J. Partee, E. L. Frankevich, B. Uhlhorn, J. Shinar, Y. Ding, T. J. Barton, *Phys. Rev. Lett.* **1999**, *82*, 3673–3676.
[18] W. Li, Y. Pan, R. Xiao, Q. Peng, S. Zhang, D. Ma, F. Li, F. Shen, Y. Wang, B. Yang, Y. Ma, *Adv. Funct. Mater.* **2014**, *24*, 1609–1614.
[19] D. Chaudhuri, E. Sigmund, A. Meyer, L. Röck, P. Klemm, S. Lautenschlager, A. Schmid, S. R. Yost, T. Van Voorhis, S. Bange, S. Höger, J. M. Lupton, *Angew. Chem. Int. Ed.* **2013**, *52*, 13449–13452; *Angew. Chem.* **2013**, *125*, 13691–13694.
[20] H. Yersin, *Highly Efficient OLEDs*, Wiley-VCH Verlag GmbH & Co. KGaA, Weinheim, Germany, **2018**.
[21] M. J. Leitl, D. M. Zink, A. Schinabeck, T. Baumann, D. Volz, H. Yersin, *Top. Curr. Chem.* **2016**, *374*, 25.
[22] F. Dumur, *Org. Electron.* **2015**, *21*, 27–39.
[23] Y. Liu, S.-C. Yiu, C.-L. Ho, W.-Y. Wong, *Coord. Chem. Rev.* **2018**, *375*, 514–557.
[24] L. Bergmann, D. M. Zink, S. Bräse, T. Baumann, D. Volz, *Top. Curr. Chem. (Z)* **2016**, *374*, 22.
[25] C. L. Linfoot, M. J. Leitl, P. Richardson, A. F. Rausch, O. Chepelin, F. J. White, H. Yersin, N. Robertson, *Inorg. Chem.* **2014**, *53*, 10854–10861.
[26] C. Bizzarri, F. Hundemer, J. Busch, S. Bräse, *Polyhedron* **2018**, *140*, 51–66.
[27] C. W. Tang, S. A. Van Slyke, *Appl. Phys. Lett.* **1987**, *51*, 913–915.
[28] C. Adachi, M. A. Baldo, S. R. Forrest, M. E. Thompson, *Appl. Phys. Lett.* **2000**, *77*, 904–906.
[29] C. Adachi, M. A. Baldo, M. E. Thompson, S. R. Forrest, *J. Appl. Phys.* **2001**, *90*, 5048–5051.
[30] J. A. G. Williams, in: *Photochemistry and Photophysics of Coordination Compounds II* (Eds.: V. Balzani, S. Campagna), Springer, Berlin, Heidelberg, **2007**, pp. 205–268.
[31] D. Ma, C. Zhang, Y. Qiu, L. Duan, *Org. Electron.* **2017**, *42*, 194–202.
[32] Y.-L. Tung, S.-W. Lee, Y. Chi, Y.-T. Tao, C.-H. Chien, Y.-M. Cheng, P.-T. Chou, S.-M. Peng, C.-S. Liu, *J. Mater. Chem.* **2005**, *15*, 460–460.
[33] M. Mauro, C.-H. Yang, C.-Y. Shin, M. Panigati, C.-H. Chang, G. D'Alfonso, L. De Cola, *Adv. Mater.* **2012**, *24*, 2054–2058.
[34] J. C. Deaton, S. C. Switalski, D. Y. Kondakov, R. H. Young, T. D. Pawlik, D. J. Giesen, S. B. Harkins, A. J. M. Miller, S. F. Mickenberg, J. C. Peters, *J. Am. Chem. Soc.* **2010**, *132*, 9499–9508.
[35] S. B. Harkins, J. C. Peters, *J. Am. Chem. Soc.* **2005**, *127*, 2030–2031.
[36] D. Volz, Y. Chen, M. Wallesch, R. Liu, C. Fléchon, D. M. Zink, J. Friedrichs, H. Flügge, R. Steininger, J. Göttlicher, C. Heske, L. Weinhardt, S. Bräse, F. So, T. Baumann, *Adv. Mater.* **2015**, *27*, 2538–2543.
[37] M. Osawa, I. Kawata, R. Ishii, S. Igawa, M. Hashimoto, M. Hoshino, *J. Mater. Chem. C* **2013**, *1*, 4375–4375.
[38] A. Schinabeck, N. Rau, M. Klein, J. Sundermeyer, H. Yersin, *Dalton Trans.* **2018**, *47*, 17067–17076.
[39] C. Förster, K. Heinze, *Chem. Soc. Rev.* **2020**, *49*, 1057–1070.
[40] D. Felder, J.-F. Nierengarten, F. Barigelletti, B. Ventura, N. Armaroli, *J. Am. Chem. Soc.* **2001**, *123*, 6291–6299.
[41] R. M. Everly, D. R. McMillin, *Photochem. Photobiol.* **1989**, *50*, 711–716.
[42] S. Keller, A. Pertegás, G. Longo, L. Martínez, J. Cerdá, J. M. Junquera-Hernández, A. Prescimone, E. C. Constable, C. E. Housecroft, E. Ortí, H. J. Bolink, *J. Mater. Chem. C* **2016**, *4*, 3857–3871.
[43] F. Brunner, L. Martínez-Sarti, S. Keller, A. Pertegás, A. Prescimone, E. C. Constable, H. J. Bolink, C. E. Housecroft, *Dalton Trans.* **2016**, *45*, 15180–15192.
[44] I. Andrés-Tomé, J. Fyson, F. B. Dias, A. P. Monkman, G. Iacobellis, P. Coppo, *Dalton Trans.* **2012**, *41*, 8669–8674.
[45] M. Osawa, M. Hoshino, M. Hashimoto, I. Kawata, S. Igawa, M. Yashima, *Dalton Trans.* **2015**, *44*, 8369–8378.
[46] M. J. Leitl, V. A. Krylova, P. I. Djurovich, M. E. Thompson, H. Yersin, *J. Am. Chem. Soc.* **2014**, *136*, 16032–16038.
[47] M. Olaru, E. Rychagova, S. Ketkov, Y. Shynkarenko, S. Yakunin, M. V. Kovalenko, A. Yablonskiy, B. Andreev, F. Kleemiss, J. Beckmann, M. Vogt, *J. Am. Chem. Soc.* **2020**, *142*, 373–381.
[48] K. Tsuge, Y. Chishina, H. Hashiguchi, Y. Sasaki, M. Kato, S. Ishizaka, N. Kitamura, *Coord. Chem. Rev.* **2016**, *306*, 636–651.
[49] M. Gernert, L. Balles-Wolf, F. Kerner, U. Müller, A. Schmiedel, M. Holzapfel, C. M. Marian, J. Pflaum, C. Lambert, A. Steffen, *J. Am. Chem. Soc.* **2020**, *142*, 8897–8909.
[50] R. Hamze, J. L. Peltier, D. Sylvinson, M. Jung, J. Cardenas, R. Haiges, M. Soleilhavoup, R. Jazzar, P. I. Djurovich, G. Bertrand, M. E. Thompson, *Science* **2019**, *363*, 601–606.
[51] M. Iwamura, H. Watanabe, K. Ishii, S. Takeuchi, T. Tahara, *J. Am. Chem. Soc.* **2011**, *133*, 7728–7736.
[52] L. X. Chen, G. B. Shaw, I. Novozhilova, T. Liu, G. Jennings, K. Attenkofer, G. J. Meyer, P. Coppens, *J. Am. Chem. Soc.* **2003**, *125*, 7022–7034.
[53] V. A. Krylova, P. I. Djurovich, B. L. Conley, R. Haiges, M. T. Whited, T. J. Williams, M. E. Thompson, *Chem. Commun.* **2014**, *50*, 7176–7179.
[54] M. Osawa, *Chem. Commun.* **2014**, *50*, 1801–1803.
[55] R. Czerwieniec, M. J. Leitl, H. H. H. Homeier, H. Yersin, *Coord. Chem. Rev.* **2016**, *325*, 2–28.
[56] B.-H. Lin, Y.-C. Wu, J.-F. Lee, M.-T. Tang, W.-F. Hsieh, *Appl. Phys. Lett.* **2019**, *114*, 091102.
[57] B.-H. Lin, Y.-C. Wu, H.-Y. Chen, S.-C. Tseng, J.-X. Wu, X.-Y. Li, B.-Y. Chen, C.-Y. Lee, G.-C. Yin, S.-H. Chang, M.-T. Tang, W.-F. Hsieh, *Opt. Express* **2018**, *26*, 2731–2739.
[58] A. Jürgensen, *Can. J. Chem.* **2017**, *95*, 1198–1204.
[59] X. Zhang, G. Smolentsev, J. Guo, K. Attenkofer, C. Kurtz, G. Jennings, J. V. Lockard, A. B. Stickrath, L. X. Chen, *J. Phys. Chem. Lett.* **2011**, *2*, 628–632.
[60] S. Lam, F. Helgl, P.-S. G. Kim, T. K. Sham, R. A. Gordon, D. Brewe, T. Regier, I. Coulthard, R. I. R. Blyth, *AIP Conf. Proc.* **2007**, *882*, 687.
[61] Y. Hu, A. Maclennan, T. K. Sham, *J. Lumin.* **2015**, *166*, 143–147.
[62] F. Heigl, S. Lam, T. Regier, I. Coulthard, T.-K. Sham, *J. Am. Chem. Soc.* **2006**, *128*, 3906–3907.
[63] T. K. Sham, *J. Electron Spectrosc. Relat. Phenom.* **2015**, *204*, 196–207.

[64] H. Shahroosvand, L. Najafi, A. Sousaraei, E. Mohajerani, M. Janghouri, F. Bonaccorso, *J. Phys. Chem. C* **2016**, *120*, 24965–24972.
[65] T. K. Sham, P. S. G. Kim, S. Lam, X. T. Zhou, R. A. Rosenberg, G. K. Shenoy, F. Heigl, A. Jürgensen, T. Regier, I. Coulthard, L. Zuin, Y.-F. Hu, in *SRMS-5 Conference*, **2006**, p. 112.
[66] P. S. G. Kim, S. J. Naftel, T. K. Sham, I. Coulthard, Y. F. Hu, A. Moewes, J. W. Freeland, *J. Electron Spectrosc. Relat. Phenom.* **2005**, *144*, 901–904.
[67] J. Goulon, P. Tola, M. Lemonnier, J. Dexpert-Ghys, *Chem. Phys.* **1983**, *78*, 347–356.
[68] S. Emura, S. Masunaga, *Phys. Rev. B* **1994**, *49*, 849–853.
[69] M. V. dos S. Rezende, P. J. R. Montes, A. B. Andrade, Z. S. Macedo, M. E. G. Valerio, *Phys. Chem. Chem. Phys.* **2016**, *18*, 17646–17654.
[70] J. J. Rehr, R. C. Albers, *Rev. Mod. Phys.* **2000**, *72*, 621–654.
[71] S. De Beer George, T. Petrenko, F. Neese, *J. Phys. Chem. A* **2008**, *112*, 12936–12943.
[72] I. Alperovich, G. Smolentsev, D. Moonshiram, J. W. Jurss, J. J. Concepcion, T. J. Meyer, A. Soldatov, Y. Pushkar, *J. Am. Chem. Soc.* **2011**, *133*, 15786–15794.
[73] S. A. Guda, A. A. Guda, M. A. Soldatov, K. A. Lomachenko, A. L. Bugaev, C. Lamberti, W. Gawelda, C. Bressler, G. Smolentsev, A. V. Soldatov, Y. Joly, *J. Chem. Theory Comput.* **2015**, *11*, 4512–4521.
[74] Y. Joly, *Phys. Rev. B* **2001**, *63*, 125120.
[75] M. Tromp, A. J. Dent, J. Headspith, T. L. Easun, X.-Z. Sun, M. W. George, O. Mathon, G. Smolentsev, M. L. Hamilton, J. Evans, *J. Phys. Chem. B* **2013**, *117*, 7381–7387.
[76] M. Chergui, E. Collet, *Chem. Rev.* **2017**, *117*, 11025–11065.
[77] Y. Hu, C. Gao, Y. Xiong, *Solar RRL* **2021**, *5*, 2000468.
[78] G. Smolentsev, V. Sundström, *Coord. Chem. Rev.* **2015**, *304–305*, 117–132.
[79] P. Glatzel, U. Bergmann, *Coord. Chem. Rev.* **2005**, *249*, 65–95.
[80] U. Bergmann, J. Kern, R. W. Schoenlein, P. Wernet, V. K. Yachandra, J. Yano, *Nat. Rev. Phys.* **2021**, *3*, 264–282.
[81] C. J. Pollock, S. DeBeer, *Acc. Chem. Res.* **2015**, *48*, 2967–2975.
[82] F. A. Lima, C. J. Milne, D. C. V. Amarasinghe, M. H. Rittmann-Frank, R. M. van der Veen, M. Reinhard, V.-T. Pham, S. Karlsson, S. L. Johnson, D. Grolimund, C. Borca, T. Huthwelker, M. Janousch, F. van Mourik, R. Abela, M. Chergui, *Rev. Sci. Instrum.* **2011**, *82*, 063111.
[83] A. M. March, A. Stickrath, G. Doumy, E. P. Kanter, B. Krässig, S. H. Southworth, K. Attenkofer, C. A. Kurtz, L. X. Chen, L. Young, *Rev. Sci. Instrum.* **2011**, *82*, 073110.
[84] G. Smolentsev, A. A. Guda, M. Janousch, C. Frieh, G. Jud, F. Zamponi, M. Chavarot-Kerlidou, V. Artero, J. A. van Bokhoven, M. Nachtegaal, *Faraday Discuss.* **2014**, *171*, 259–273.
[85] C. Bressler, C. Milne, V.-T. Pham, A. ElNahhas, R. M. van der Veen, W. Gawelda, S. Johnson, P. Beaud, D. Grolimund, M. Kaiser, C. N. Borca, G. Ingold, R. Abela, M. Chergui, *Science* **2009**, *323*, 489–492.
[86] S. Khan, F. Bahnsen, S. Cramm, S. Döring, J. Grewe, M. Höner, H. Huck, M. Huck, R. Molo, L. Plucinski, A. Schick, C. M. Schneider, P. Ungelenk, *Synchrotron Radiation News* **2013**, *26*, 25–29.
[87] J. Li, X. Ren, Y. Yin, K. Zhao, A. Chew, Y. Cheng, E. Cunningham, Y. Wang, S. Hu, Y. Wu, M. Chini, Z. Chang, *Nat. Commun.* **2017**, *8*, 186.
[88] G. C. O'Neil, L. Miaja-Avila, Y. I. Joe, B. K. Alpert, M. Balasubramanian, D. M. Sagar, W. Doriese, J. W. Fowler, W. K. Fullagar, N. Chen, G. C. Hilton, R. Jimenez, B. Ravel, C. D. Reintsema, D. R. Schmidt, K. L. Silverman, D. S. Swetz, J. Uhlig, J. N. Ullom, *J. Phys. Chem. Lett.* **2017**, *8*, 1099–1104.
[89] B. Mahieu, N. Jourdain, K. T. Phuoc, F. Dorchies, J.-P. Goddet, A. Lifschitz, P. Renaudin, L. Lecherbourg, *Nat. Commun.* **2018**, *9*, 3276.
[90] J. R. Kirchhoff, R. E. Gamache, M. W. Blaskie, A. A. Del Paggio, R. K. Lengel, D. R. McMillin, *Inorg. Chem.* **1983**, *22*, 2380–2384.
[91] L. X. Chen, G. Jennings, T. Liu, D. J. Gosztola, J. P. Hessler, D. V. Scaltrito, G. J. Meyer, *J. Am. Chem. Soc.* **2002**, *124*, 10861–10867.
[92] T. J. Penfold, S. Karlsson, G. Capano, F. A. Lima, J. Rittmann, M. Reinhard, M. H. Rittmann-Frank, O. Braem, E. Baranoff, R. Abela, I. Tavernelli, U. Rothlisberger, C. J. Milne, M. Chergui, *J. Phys. Chem. A* **2013**, *117*, 4591–4601.
[93] G. Smolentsev, A. V. Soldatov, L. X. Chen, *J. Phys. Chem. A* **2008**, *112*, 5363–5367.
[94] M. Rentschler, S. Iglesias, M.-A. Schmid, C. Liu, S. Tschierlei, W. Frey, X. Zhang, M. Karnahl, D. Moonshiram, *Chem. Eur. J.* **2020**, *26*, 9527–9536.
[95] K. A. Fransted, N. E. Jackson, R. Zong, M. W. Mara, J. Huang, M. R. Harpham, M. L. Shelby, R. P. Thummel, L. X. Chen, *J. Phys. Chem. A* **2014**, *118*, 10497–10506.
[96] M. S. Kelley, M. L. Shelby, M. W. Mara, K. Haldrup, D. Hayes, R. G. Hadt, X. Zhang, A. B. Stickrath, R. Ruppert, J.-P. Sauvage, D. Zhu, H. T. Lemke, M. Chollet, G. C. Schatz, L. X. Chen, *J. Phys. B* **2017**, *50*, 154006.
[97] M. W. Mara, K. A. Fransted, L. X. Chen, *Coord. Chem. Rev.* **2015**, *282–283*, 2–18.
[98] A. Guda, J. Windisch, B. Probst, J. A. van Bokhoven, R. Alberto, M. Nachtegaal, L. X. Chen, G. Smolentsev, *Phys. Chem. Chem. Phys.* **2021**, *23*, 26729–26736.
[99] D. Moonshiram, P. Garrido-Barros, C. Gimbert-Suriñach, A. Picón, C. Liu, X. Zhang, M. Karnahl, A. Llobet, *Chem. Eur. J.* **2018**, *24*, 6464–6472.
[100] F. de Groot, *Chem. Rev.* **2001**, *101*, 1779–1808.
[101] G. Smolentsev, C. J. Milne, A. Guda, K. Haldrup, J. Szlachetko, N. Azzaroli, C. Cirelli, G. Knopp, R. Bohinc, S. Menzi, G. Pamfilidis, D. Gashi, M. Beck, A. Mozzanica, D. James, C. Bacellar, G. F. Mancini, A. Tereshchenko, V. Shapovalov, W. M. Kwiatek, J. Czapla-Masztafiak, A. Cannizzo, M. Gazzetto, M. Sander, M. Levantino, V. Kabanova, E. Rychagova, S. Ketkov, M. Olaru, J. Beckmann, M. Vogt, *Nat. Commun.* **2020**, *11*, 2131.
[102] J.-H. Lee, C.-H. Chen, P.-H. Lee, H.-Y. Lin, M. Leung, T.-L. Chiu, C.-F. Lin, *J. Mater. Chem. C* **2019**, *7*, 5874–5888.
[103] M. A. Baldo, C. Adachi, S. R. Forrest, *Phys. Rev. B* **2000**, *62*, 10967–10977.
[104] G. Smolentsev, K. M. van Vliet, N. Azzaroli, J. A. van Bokhoven, A. M. Brouwer, B. de Bruin, M. Nachtegaal, M. Tromp, *Photochem. Photobiol. Sci.* **2018**, *17*, 896–902.
[105] K. Hämäläinen, D. P. Siddons, J. B. Hastings, L. E. Berman, *Phys. Rev. Lett.* **1991**, *67*, 2850–2853.
[106] A. Britz, S. I. Bokarev, T. A. Assefa, È. G. Bajnóczi, Z. Németh, G. Vankó, N. Rockstroh, H. Junge, M. Beller, G. Doumy, A. M. March, S. H. Southworth, S. Lochbrunner, O. Kühn, C. Bressler, W. Gawelda, *ChemPhysChem* **2021**, *22*, 693–700.
[107] D. Goeries, B. Dicke, P. Roedig, N. Stuebe, J. Meyer, A. Galler, W. Gawelda, A. Britz, P. Gessler, H. S. Namin, A. Beckmann, M. Schlie, M. Warmer, M. Naumova, C. Bressler, M. Ruebhausen, E. Weckert, A. Meents, *Rev. Sci. Instrum.* **2016**, *87*, 053116.
[108] M. Sarma, W.-L. Tsai, W.-K. Lee, Y. Chi, C.-C. Wu, S.-H. Liu, P.-T. Chou, K.-T. Wong, *Chem* **2017**, *3*, 461–476.
[109] D. Jacquemin, D. Escudero, *Chem. Sci.* **2017**, *8*, 7844–7850.
[110] E. Borfecchia, C. Garino, D. Gianolio, L. Salassa, R. Gobetto, C. Lamberti, *Catal. Today* **2014**, *229*, 34–45.
[111] K. S. Kjær, T. B. V. Driel, T. C. B. Harlang, K. Kunnus, E. Biasin, K. Ledbetter, R. W. Hartsock, M. E. Reinhard, S. Koroidov, L. Li, M. G. Laursen, F. B. Hansen, P. Vester, M. Christensen, K. Haldrup, M. M. Nielsen, A. O. Dohn, M. I. Pápai, K. B. Møller, P. Chabera, Y. Liu, H. Tatsuno, C. Timm, M. Jarenmark, J. Uhlig, V. Sundstöm, K. Wärnmark, P. Persson, Z. Németh, D. S. Szemes, É. Bajnóczi, G. Vankó, R. Alonso-Mori, J. M. Glownia, S. Nelson, M. Sikorski, D. Sokaras, S. E. Canton, H. T. Lemke, K. J. Gaffney, *Chem. Sci.* **2019**, *10*, 5749–5760.
[112] H. Tatsuno, K. S. Kjær, K. Kunnus, T. C. B. Harlang, C. Timm, M. Guo, P. Chàbera, L. A. Fredin, R. W. Hartsock, M. E. Reinhard, S. Koroidov, L. Li, A. A. Cordones, O. Gordivska, O. Prakash, Y. Liu, M. G. Laursen, E. Biasin, F. B. Hansen, P. Vester, M. Christensen, K. Haldrup, Z. Németh, D. S. Szemes, É. Bajnóczi, G. Vankó, T. B. V. Driel, R. Alonso-Mori, J. M. Glownia, S. Nelson, M. Sikorski, H. T. Lemke, D. Sokaras, S. E. Canton, A. O. Dohn, K. B. Møller, M. M. Nielsen, K. J. Gaffney, K. Wärnmark, V. Sundström, P. Persson, J. Uhlig, *Angew. Chem. Int. Ed.* **2020**, *59*, 364–372; *Angew. Chem.* **2020**, *132*, 372.
[113] E. Fabbri, D. F. Abbott, M. Nachtegaal, T. J. Schmidt, *Curr. Opin. Electrochem.* **2017**, *5*, 20–26.
[114] F. Lin, Y. Liu, X. Yu, L. Cheng, A. Singer, O. G. Shpyrko, H. L. Xing, N. Tamura, C. Tian, T.-C. Weng, X.-Q. Yang, Y. S. Meng, D. Nordlund, W. Yang, M. M. Doeff, *Chem. Rev.* **2017**, *117*, 13123–13186.
[115] S.-M. Bak, Z. Shadike, R. Lin, X. Yu, X.-Q. Yang, *NPG Asia Mater.* **2018**, *10*, 563–580.

Manuscript received: August 22, 2021
Revised manuscript received: November 24, 2021
Version of record online: January 12, 2022